

# PC-Droid: Faster diffusion and improved quality for particle cloud generation

Matthew Leigh,<sup>\*</sup> Debajyoti Sengupta,<sup>†</sup> John Andrew Raine,<sup>‡</sup> Guillaume Quétant, and Tobias Golling

*Département de physique nucléaire et corpusculaire, University of Geneva, Switzerland*

Building on the success of PC-JeDi we introduce PC-Droid, a substantially improved diffusion model for the generation of jet particle clouds. By leveraging a new diffusion formulation, studying more recent integration solvers, and training on all jet types simultaneously, we are able to achieve state-of-the-art performance for all types of jets across all evaluation metrics. We study the trade-off between generation speed and quality by comparing two attention based architectures, as well as the potential of consistency distillation to reduce the number of diffusion steps. Both the faster architecture and consistency models demonstrate performance surpassing many competing models, with generation time up to two orders of magnitude faster than PC-JeDi.

## I. INTRODUCTION

An incredible amount of computing resources is required to keep up with demands for simulated events at the intensity frontier of high energy physics (HEP). As such, focus has turned to fast surrogate models for event and detector simulation. Deep generative models and modern machine learning techniques have shown great promise in improving the fidelity and speed of fast simulation approaches [1–25]. Recently, diffusion models have come to the fore in a wide range of disciplines, notably for images generation [26–31]. However, they have also demonstrated promise in applications in HEP for fast detector simulation [32–34], the generation of jets [35–37], unfolding [38], and anomaly detection [39].

The recent rise of diffusion models has also lead to a rapid development of approaches [40], similar to the development observed in generative adversarial networks [41]. As such, the level of performance is continuously improving with more stable training procedures and improved differential equation solvers for generation.

In this work we introduce PC-Droid (Particle Cloud Diffusion of reconstructed objects with improved denois-

ing), a significant improvement over the PC-JeDi approach introduced in Ref. [35], demonstrating both a decreased inference time and higher-fidelity generation. We use a more recently developed formulation for diffusion models [31] and combine it with improved diffusion sampling algorithms [42, 43]. We compare and contrast different network architectures, balancing the overall performance against generation time. Furthermore, in an effort to greatly reduce the generation time, we study the quality of consistency models [44] for jet generation.

With PC-Droid we achieve state-of-the-art performance as measured on standard metrics, as well as a new set of benchmarks. The repository<sup>1</sup> used in this work is publicly available.

## II. METHOD

PC-Droid is a family of models which are trained to generate the constituent particles of jets either conditionally, given the desired kinematics of the jet, or unconditionally, with jet kinematics sampled from distributions learned from the training dataset.

<sup>\*</sup> matthew.leigh@unige.ch

<sup>†</sup> debajyoti.sengupta@unige.ch

<sup>‡</sup> john.raine@unige.ch

<sup>1</sup> <https://github.com/rodem-hep/pcdroid>

### A. Improved diffusion formulation

One of the key developments in PC-Droid is the change in diffusion paradigm and setup. PC-Droid follows the ‘EDM’ noise scheduler and network preconditioning from Ref. [31]. This introduces several crucial changes.

First, following the notation from Ref. [35], the signal and noise rates are set to  $\gamma(t) = 1$  and  $\sigma(t) = t$ . This simplifies the stochastic differential equation (SDE) to

$$dx_t = \sqrt{2t} dw,$$

with the corresponding reverse ordinary differential equation (ODE) reducing to

$$dx_t = -t \nabla_x \log p(x; t).$$

Consequently, the ODE has solutions with straighter trajectories. This results in fewer truncation errors during generation compared to the previous variance preserving approach. The significant benefit of this change is being able to perform the reverse diffusion process in fewer steps. In addition,  $t$  and  $\sigma$  are now interchangeable, with  $t$  no longer bounded between 0 and 1 and instead in the range  $t = \sigma \in [0, 80]$ .

Second, during training we sample the noise rates using a log-norm distribution defined by  $\log(\sigma) \sim \mathcal{N}(-1.2, 1.2)$ . At low values of  $\sigma$ , the magnitude of the artificial noise added to the samples approaches the natural stochasticity in the data. At high values of  $\sigma$ , the denoising targets produce an estimator of the score function with excessively high variance. The log-norm sampling adds focus to intermediate values of  $\sigma$ , where the most gain in performance is possible. The sampling distribution is taken from Ref. [31], and is found to be similarly optimal for our application.

Third, smarter skip and scaling connections are introduced to the network architecture. The variables  $c_{in}(\sigma)$ ,  $c_{out}(\sigma)$  and  $c_{skip}(\sigma)$  are all parametrised by the noise strength  $\sigma$ , and are combined for the denoised estimate

$$D_\theta(\mathbf{x}; \sigma, \mathbf{y}) = c_{out} F_\theta(c_{in} \mathbf{x}; \sigma, \mathbf{y}) + c_{skip} \mathbf{x},$$

where  $F_\theta$  is the prediction from the network for the input point cloud  $\mathbf{x}$  and conditional parameters  $\mathbf{y}$ . As the variance is no longer preserved during the diffusion process, the scaling functions are used to maintain the unit variance of the raw inputs and outputs of the network. The skip connection allows the  $\mathbf{x}$  to bypass the network at low  $\sigma$ , as the input is closer to the target.

Finally, this new framework results in a change to the objective function of the network. Here, the loss is calculated from the distance between the denoised output and the true target  $\mathbf{x}_0$

$$\mathcal{L} = \|D_\theta(\mathbf{x}; \sigma, \mathbf{y}) - \mathbf{x}_0\|_2^2,$$

where previously, the loss was calculated from the difference in the predicted noise added in  $\mathbf{x}$ .

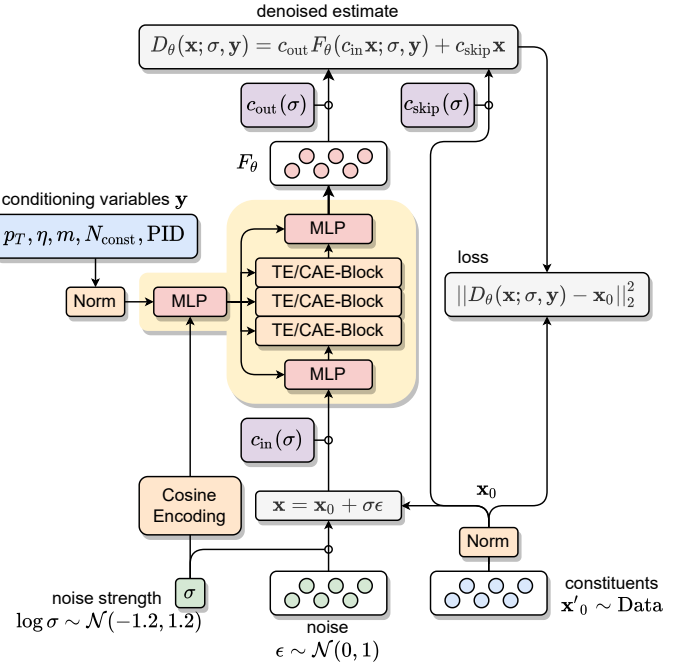


FIG. 1: PC-Droid network architecture and training setup.

The general PC-Droid architecture and the training process is shown in Fig. 1.

Another key development has been in the choice of integration solvers used during inference. Several state-of-the-art algorithms have been studied including those

provided by `k-diffusion` library.<sup>2</sup> The most promising solvers are presented in this work.

In PC-JeDi dedicated models were trained for each jet type; in PC-Droid a single conditional model for all five particle types (PID) ( $q$  - light quark;  $g$  - gluon;  $t$  - top quark;  $W$  -  $W$  boson;  $Z$  -  $Z$  boson) is produced. By training simultaneously on all jet types for a single conditional model, we are able to increase the overall training statistics for the PC-Droid model. This is observed to result in improved generation quality for all jet types in comparison to individual models trained separately for each.

## B. Model training

A denoising transformer is trained for each of the JetNet datasets introduced in Ref. [45] comprising of up to 30 [46] and 150 [47] constituents. To allow comparisons to PC-JeDi, the optimizer, learning rate scheduler, and most of the hyperparameters are left unchanged. The only notable changes are the reduction in the number of transformer encoder layers from four to three, and the inclusion of an extra MLP to combine the cosine embedding of  $\sigma$  with the context vector. For the 150 constituents model we double the token dimension and the width of the MLP layers. As in PC-JeDi, each jet constituent is represented by its coordinates relative to the jet centre  $\Delta\eta$  and  $\Delta\phi$ , and its transverse momentum of the form  $\log(p_T + 1)$ .

## C. Cross-attention encoder

In PC-JeDi only a self-attention transformer encoder (TE) architecture was studied which, although very expressive, is computationally expensive. The number of operations scales with  $\mathcal{O}(N_{const}^2)$  for the number of constituents  $N_{const}$ . As diffusion models require many network passes during generation, this makes self-attention

a suboptimal choice for fast generation. For the 30 constituent models this does not present a large problem, however when moving to 150 constituents the impact is non-negligible. Therefore, in addition to the transformer model we also introduce the cross-attention encoder (CAE) as a faster and more memory efficient permutation equivariant network.

A schematic overview of the CAE-Block is shown in Fig. 2. In a CAE-Block, the input point cloud is used to update a single global token using multi-headed cross-attention. The global token is then further updated using a residual multi-layer perceptron (MLP), before being re-distributed back to the point cloud using another cross-attention layer and a residual MLP update. This process of global pooling followed by distribution can be thought of as a transformer analogue to EPiC layers [48]. We construct the full CAE by stacking together multiple CAE-Blocks in sequence, and allowing the initial global token to be fully learnable. The number of attention operations for the CAE scales with  $\mathcal{O}(2N_{const})$ .

We produced a CAE based version of PC-Droid on the 150 dataset using the same training setup, model dimension, and number of layers as the baseline transformer for a fair comparison.

## D. Consistency models

In this work we investigate the process of consistency distillation (CD) [44], whereby a teacher network is used to train a student network in order to solve the reverse diffusion process in less time steps, even enabling *one-shot* generation. The teacher network in this case is a standard diffusion model which can already be used in conjunction with an integration method to solve the reverse diffusion ODE [49].

During training, the objective of the student network is to map all points sampled along a same ODE trajectory to the same output. To ensure that the student model does not collapse to a constant function, a boundary con-

<sup>2</sup> <https://github.com/crowsonkb/k-diffusion/tree/v0.0.15>

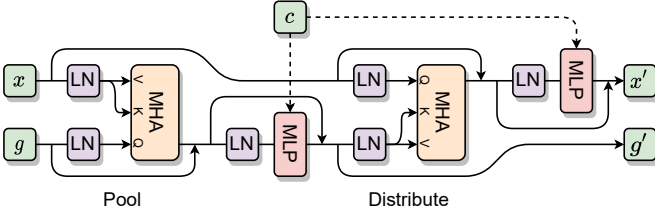


FIG. 2: A single cross-attention encoder block updating both an input point cloud  $x$  and a global token  $g$ , using layer-norm (LN), multi-headed attention (MHA).

Converging arrows represent vector additional and contextual information  $c$  is injected into the network by concatenating to the inputs of the MLPs. The first attention operation effectively pools information from the point cloud into the global token. The second attention operation is inverted, and information from the updated global token is distributed back to the point cloud.

dition is enforced such that the it approaches the identity map as  $\sigma$  approaches zero. We follow the approach in Ref. [44] and use skip connections to enforce this. This boundary condition means that the global minimum of the training loss is reached only when the student network learns to map each point of the ODE trajectory to its endpoint.

At the start of training the student model is initialised with the same parameter values as the teacher model. During training, two adjacent points on the ODE are sampled using the teacher network and sampler, and are subsequently evaluated with the student. The training loss is the mean squared distance between these two outputs. To stabilize training, the student network is duplicated into a online and target network, a process commonly found in deep reinforcement learning [50, 51]. Gradients are only propagated through the online network which always processes the ODE sample with the larger  $\sigma$ . After each iteration, the target network is synced with the student network using an exponentially decaying average of the parameters.

Although both are distillation methods, consistency models differ from progressive distillation models [52], such as the approach applied to jet generation in Ref. [36]. In progressive distillation, new models are iteratively trained to predict the amount of noise removed in  $N$  steps of the nominal model. This processes is repeated with each new model trained to reduce the overall number of steps required, culminating in a faster generation time. No information about the ODE trajectories are required, only the total amount of noise removed after  $N$  steps.

### E. Unconditional generation

PC-Droid is trained as a conditional generative model, with the jet kinematics  $(p_T, \eta, m)$ , the number of constituents ( $N_{const}$ ), and the PID used as conditions. To allow for unconditional generation we present a method using normalizing flows [53] to generate these variables as an initial step.

One normalizing flow (Flow-*vecp*) is trained to learn the probability density  $p(p_T, \eta, m, N_{const} | \text{PID})$ . The transformer diffusion models are parametrised by the number of constituents, and therefore this value is always required at generation time. The number of constituents is correlated to many of the jet properties, and thus we require a normalizing flow to learn these correlations. A second conditional normalizing flow (Flow- $N$ ) is trained to learn the probability density  $p(N_{const} | p_T, \eta, m, \text{PID})$ . This second flow is designed to highlight how PC-Droid can be used as a surrogate fast simulator where one would typically know the parton type and kinematics, but not the number of particles present in the final jet.

Both flows are trained with a maximum log likelihood objective, and consist of five transformation layers using rational quadratic splines [54]. Coupling layers are used in the flow generating values for  $p(p_T, \eta, m, N_{const} | \text{PID})$ , whilst the one dimensional flow for  $p(N_{const} | p_T, \eta, m, \text{PID})$  simply learns a single spline

per layer. For both flows, a dequantisation step is used to simplify the learning of the  $N_{const}$  distribution; at inference time the generated value is rounded to the nearest integer. We use the Adam [55] optimizer with default settings with a cosine learning rate. As these distributions are not very complex, near perfect performance is obtained using only four layers and 100k learnable parameters.

This approach is preferential over implicitly unconditional models as it segments what the model needs to learn along a logical line. The kinematics of a jet is strongly correlated to and influential on its substructure, and therefore the kinematics of the individual constituents. Providing this information to the diffusion model is observed to improve the overall performance. Secondly, the kinematics can be far more easily learned and modelled with a normalizing flow than embedding it in the same network.

## F. Comparison to prior work

Diffusion models are a fast growing family of generative models, and are becoming more actively studied for their use in high energy physics. Whilst this work was being undertaken, Ref. [36] introduced a fast diffusion model for jet particle cloud generation exploiting progressive distillation. Our approach differs in that we are studying the impact of both the diffusion model architecture on generation speed, as well as the use of consistency distillation.

We are similar to FPCD in that we train on all jet types simultaneously, have a second model for generating the conditions, and can generate jets with up to 150 constituents. However, our approach differs in that we are studying the impact of both the diffusion model architecture on generation speed, as well as the use of consistency distillation. We also use a different diffusion paradigm to train and perform inference. The additional conditioning variables are also modelled differently be-

tween the two approaches. In Ref. [36] a second diffusion model is jointly trained to generate the kinematics and  $N_{const}$  of the jets given the PID. However, generating the conditional information is an orthogonal task to the constituent generation, and we find we do not need to train both jointly as there are no shared weights in the two networks. Using a normalizing flow is also significantly faster at inference than a second diffusion model, and well suited to the structured vector output. In addition, it is unlikely that a fast surrogate model will be used solely for the amplification of statistics from the training distribution and with conditional generation any desired distributions over the jet kinematics can be achieved.

Other adversarial approaches such as MPGAN [45] and EPiC-GAN [48] rely on implicitly learning the correlations to the jet kinematics without a second network. In EPiC-GAN a kernel-density estimator (KDE) is used to model the number of constituents, which is a conditional parameter of the generation and correlated to the jet invariant mass and  $p_T$ . However, the KDE does not take into account correlations between the number of constituents and the kinematics of the jet.

Conditioning is also studied in JetFlow [56], where normalizing flows are used to generate jets. Due to the nature of normalizing flows, in comparison to the diffusion and GAN based architectures, JetFlow is not permutation invariant. Furthermore, as normalizing flows have a fixed dimensionality, jets with fewer than 30 particles are zero-padded up to the maximum size. Small levels of noise added to the empty constituents during training.

Due to the fixed size of normalizing flows, jets with fewer than 30 particles are zero-padded up to the maximum size, with small levels of noise added to the empty constituents. The number of constituents, along with the jet mass, are provided to the network as conditions during training and at inference. To generate new jets with JetFlow, the conditioning variables are sampled sequentially from two cumulative distribution functions (CDF), with a separate jet mass CDF for each value of  $N_{const}$ .

Concurrent with this work, Ref. [57] studied the use of similar cross attention layers for faster particle cloud generation. A key difference between this approach and the CAE layer is the use of attention to redistribute the global token to the point cloud, which in Ref. [57] is performed with concatenation to the individual points before being fed through a linear layer.

### III. RESULTS

#### A. JetNet30

To assess the quality of the generated jets we compare distributions of several observables to the JetNet30 test set, which we label as Delphes. For a quantitative analysis, we use the metrics<sup>3</sup> introduced in Ref. [35] and Ref. [45]. For each metric we establish an ideal limit by comparing the training and test sets, which corresponds to the natural variation in the Delphes samples. All PC-Droid samples used in this study are taken from the fully conditional generation regime. We observe very little difference in performance between sampling all conditions from the normalizing flow for each jet, and taking the jet kinematics from the training data.

We test a wide variety of integration solvers in the generation stage for PC-Droid. These include a fourth order linear multistep method (LMS) [58] and DPM-Solver-2 (DPM2) [42]. We study the trade-off in quality of the generated jets and the amount of neural function evaluations (NFE) in order to choose the best solver and a corresponding optimal step size. For this comparison we look at the FPND,  $W_1^M$ , and the  $W_1^{732}$  metrics. Results for PC-JeDi are obtained using the Euler-Maruyama sampler at 200 NFE [35]. From Fig. 3, we see most solvers saturate at around 100 NFE. While there is no clearly superior method, we observe that the LMS solver per-

forms the best across most metrics and henceforth we use the LMS solver at 100 NFE for all PC-Droid results. We also find that with most solvers PC-Droid outperforms MPGAN with as few as 20 steps.

Accurately modelling individual constituents is a crucial requirement when it comes to jet generation. Figure 4 shows the  $p_T$  distributions of the leading, fifth leading, and twentieth leading constituents of the generated top and gluon jets as modelled by PC-Droid and PC-JeDi. PC-Droid demonstrates improved agreement with Delphes compared to PC-JeDi across all the constituents, especially in the tails.

Next, we look at the substructure variable distributions of the generated jets and correlations between them, which are crucial for jet tagging. We specifically look at top jets as they are the ones which have the most complex substructure and in our experience have been the hardest to model. In Fig. 5, we see that PC-Droid has a much improved  $\tau_{32}$  modelling compared to PC-JeDi, and has an excellent agreement with Delphes simulation for all other substructure variables.

The generation performance is summarised in Table I for gluon and top jets. It is observed that MPGAN and PC-JeDi already approach the ideal limit for several of the metrics introduced in Ref. [45], thus we focus on metrics where performance gain can be achieved. Particularly in FPND, PC-Droid manages to significantly bridge that gap and surpasses all methods in all metrics.

#### B. JetNet150

We extend this work to the 150 constituent dataset and in addition to the original transformer based model we also evaluate the CAE network labelled PC-Droid (CAE). We find that the LMS sampling method at 100 NFE provides a similarly optimal result for both networks on this dataset.

Substructure distributions are shown in Fig. 6. Both models do very well in capturing jet mass and  $D2$ , but

<sup>3</sup> For metrics which require bootstrapping, we use 16 batches of 20000 events for all methods.

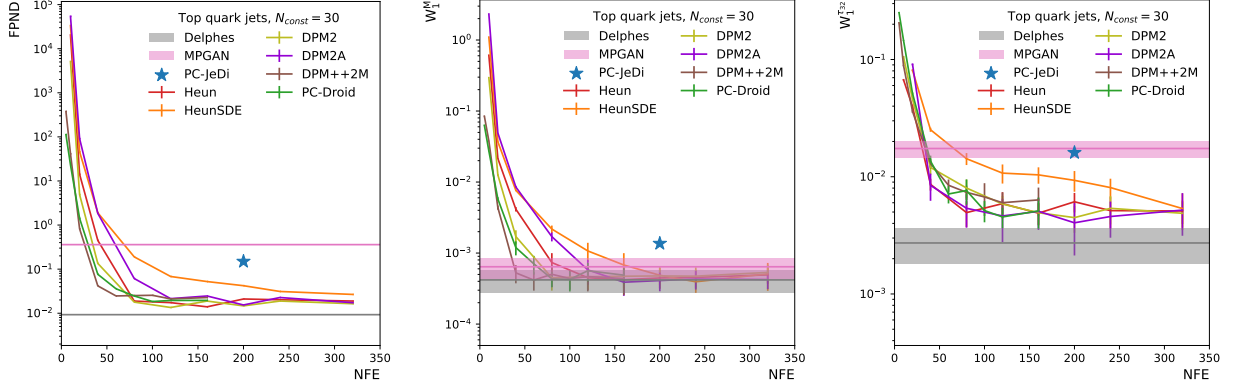


FIG. 3: Performance as measured by FPND (left),  $W_1^M$  (middle), and  $W_1^{T_{32}}$  (right) on the NFE for top jets with up to 30 constituents. We generate samples with PC-Droid using Heun and HeunSDE methods [31], DPM2 [42], DPM2 with ancestral sampling (DPM2A), DPM++2M [43], and LMS [58].

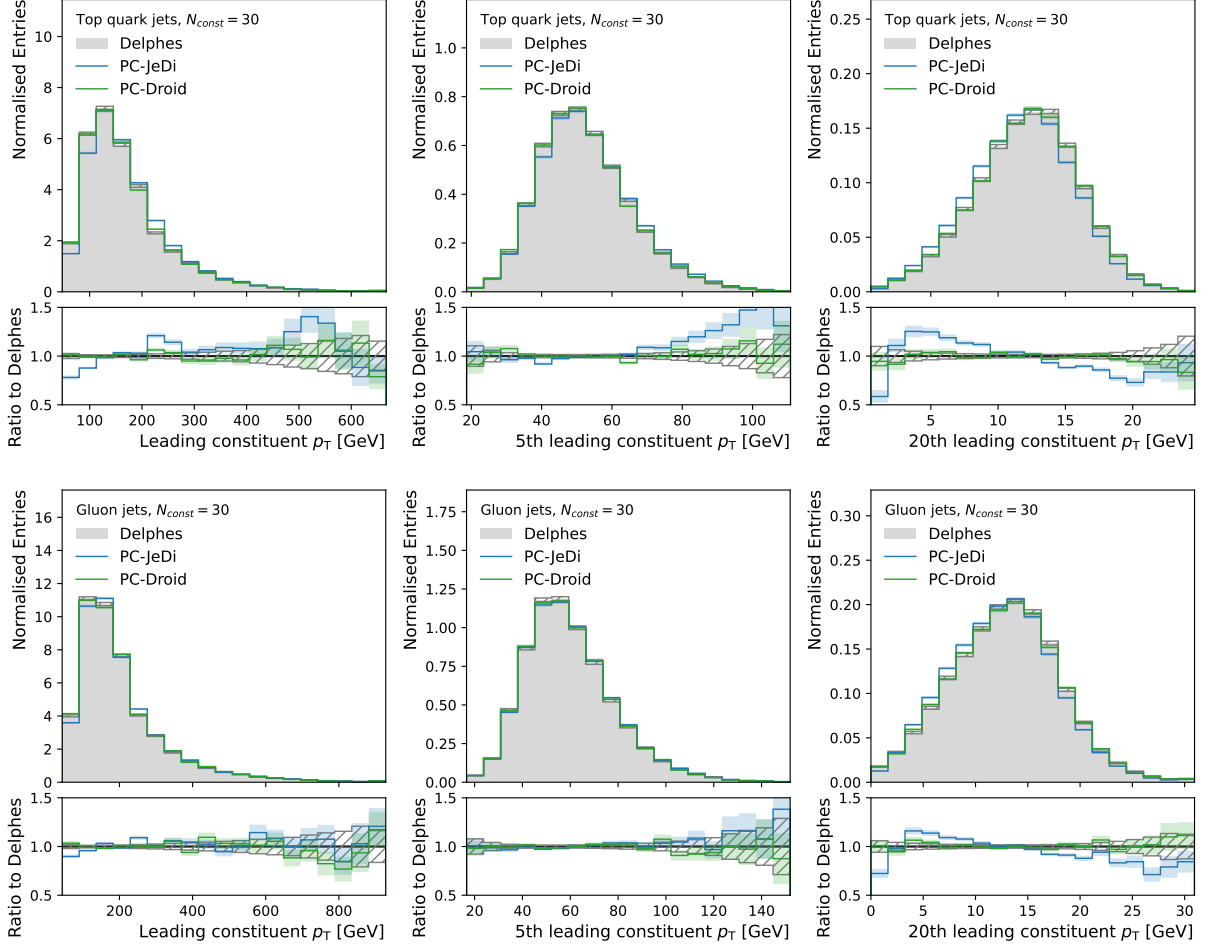


FIG. 4: Comparison of  $p_T$  distributions of the leading, fifth leading, and twentieth leading constituents of the generated top and gluon jets with up to 30 constituents.

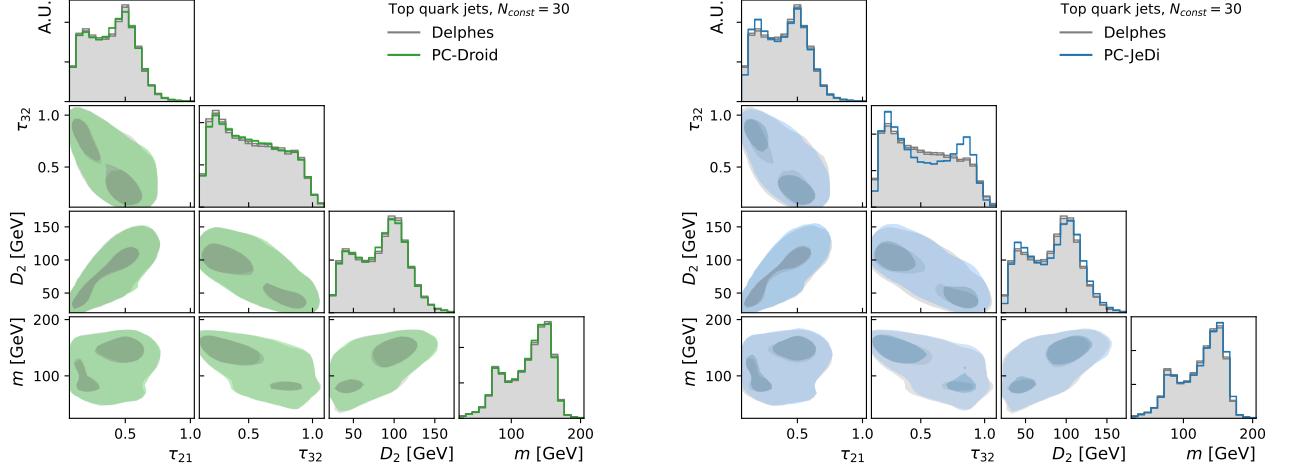


FIG. 5: Mass and substructure distributions of the generated top jets with up to 30 constituents. The diagonal consists of the marginals of the distributions and the off-diagonal elements contain the joint distributions.

TABLE I: Comparison of generative models on top and gluons with up to 30 constituents. Lower is better.

Jet	Model	FPND	$W_1^P (\times 10^{-4})$	$W_1^{EFP} (\times 10^{-6})$	$W_1^M (\times 10^{-4})$	$W_1^{\tau_{21}} (\times 10^{-3})$	$W_1^{\tau_{32}} (\times 10^{-3})$	$W_1^{D_2} (\times 10^{-1})$
Top	Delphes	0.01	$3.98 \pm 1.27$	$8.07 \pm 3.51$	$3.23 \pm 1.07$	$2.01 \pm 0.74$	$2.90 \pm 1.59$	$3.34 \pm 1.03$
	PC-Droid	<b>0.02</b>	<b><math>5.02 \pm 1.59</math></b>	<b><math>11.59 \pm 3.29</math></b>	<b><math>4.27 \pm 1.39</math></b>	<b><math>2.91 \pm 1.09</math></b>	<b><math>5.14 \pm 1.06</math></b>	<b><math>4.75 \pm 1.26</math></b>
	PC-JeDi	0.15	$12.07 \pm 2.01$	$35.61 \pm 4.92$	$13.64 \pm 3.21$	$4.55 \pm 1.16$	$16.05 \pm 1.31$	$14.12 \pm 1.48$
	MPGAN	0.36	$21.73 \pm 2.02$	$12.80 \pm 4.89$	$6.41 \pm 2.09$	$6.61 \pm 0.92$	$17.41 \pm 2.78$	$11.34 \pm 1.03$
Gluon	Delphes	0.01	$3.54 \pm 1.19$	$4.07 \pm 1.27$	$4.39 \pm 1.59$	$3.79 \pm 1.42$	$2.26 \pm 0.51$	$3.72 \pm 1.07$
	PC-Droid	<b>0.01</b>	<b><math>3.66 \pm 1.07</math></b>	<b><math>4.13 \pm 1.61</math></b>	<b><math>4.48 \pm 1.47</math></b>	<b><math>2.89 \pm 0.80</math></b>	<b><math>1.99 \pm 0.51</math></b>	<b><math>4.14 \pm 1.30</math></b>
	PC-JeDi	0.10	$5.83 \pm 1.44$	$5.68 \pm 1.09$	$5.66 \pm 1.51$	$12.48 \pm 0.98$	$13.32 \pm 0.96$	$10.70 \pm 2.60$
	MPGAN	0.13	$10.26 \pm 1.51$	$8.76 \pm 2.44$	$8.15 \pm 2.10$	$16.83 \pm 2.08$	$25.27 \pm 1.29$	$24.88 \pm 2.91$

the the quality drop between the transformer and the CAE becomes apparent when looking at the subjettness ratios. This has a detrimental effect on the correlations between substructure observables, as can be seen in Fig. 7.

We provide a quantitative comparison between the performance of the PC-Droid models and EPiC-GAN in Table II. PC-Droid with the self attention network displays superior performance in all metrics where there is notable separation between models. EPiC-GAN seems to offer superior performance in modelling the relative mass, but

all generative modes are within agreement to Delphes on this metric.

Comparing the performance of models in the context of jet tagging is also useful, as ideally a jet classifier has the same separation power on the generated and reference samples. The FPND score introduced in Ref [45] attempts to capture this, where the jet classifier is a message passing neural network. Here, we present simpler and interpretable method using a 2D cut based tagger, similar to those used by the ATLAS collaboration [59–61]. We define a simple cut based top/gluon tagger



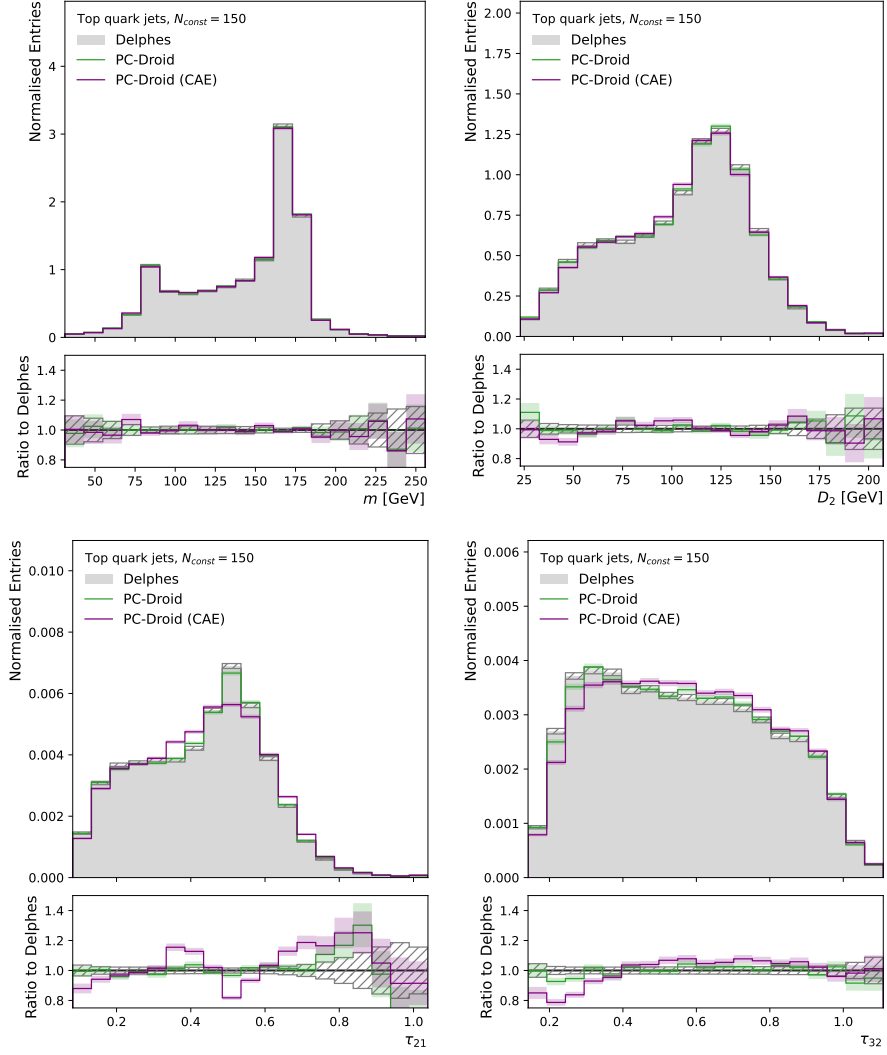


FIG. 6: Comparison of the standard transformer based PC-Droid and the cross attention encoder (CAE) variant using the generated mass and substructure marginals of top jets with up to 150 constituents.

TABLE II: Comparison of generative models on top and gluon jets with up to 150 constituents. Lower is better. The FPN score is only sensitive to the leading 30 constituents.

Jet	Model	FPND	$W_1^P (\times 10^{-4})$	$W_1^{EFP} (\times 10^{-6})$	$W_1^M (\times 10^{-4})$	$W_1^{\tau_{21}} (\times 10^{-3})$	$W_1^{\tau_{32}} (\times 10^{-3})$	$W_1^{D^2} (\times 10^{-1})$
Top	Delphes	0.01	$3.03 \pm 0.78$	$14.77 \pm 5.61$	$3.96 \pm 0.94$	$1.78 \pm 0.56$	$2.78 \pm 1.03$	$3.82 \pm 1.54$
	PC-Droid	<b>0.01</b>	$5.45 \pm 1.70$	<b><math>15.41 \pm 5.38</math></b>	<b><math>3.60 \pm 1.20</math></b>	<b><math>2.87 \pm 1.20</math></b>	<b><math>4.70 \pm 1.88</math></b>	<b><math>4.07 \pm 0.85</math></b>
	PC-Droid (CAE)	0.09	<b><math>4.93 \pm 1.58</math></b>	$17.97 \pm 4.15$	$4.72 \pm 1.93$	$6.30 \pm 1.00$	$12.94 \pm 1.42$	$6.98 \pm 1.04$
	EPiC-GAN	0.95	$36.70 \pm 1.80$	$30.29 \pm 5.01$	$6.93 \pm 1.49$	$13.28 \pm 1.80$	$37.56 \pm 1.92$	$19.03 \pm 2.40$
Gluon	Delphes	0.01	$3.88 \pm 1.24$	$10.66 \pm 3.30$	$6.04 \pm 2.18$	$2.92 \pm 1.20$	$1.74 \pm 0.45$	$4.65 \pm 1.35$
	PC-Droid	<b>0.01</b>	<b><math>3.69 \pm 1.35</math></b>	<b><math>10.30 \pm 4.36</math></b>	$5.26 \pm 2.43$	<b><math>3.13 \pm 1.10</math></b>	<b><math>2.24 \pm 0.93</math></b>	<b><math>4.81 \pm 1.27</math></b>
	PC-Droid (CAE)	0.02	$4.30 \pm 1.48$	$11.31 \pm 3.46$	$5.37 \pm 2.02$	$3.24 \pm 0.90$	$3.06 \pm 0.91$	$5.02 \pm 1.34$
	EPiC-GAN	0.54	$32.22 \pm 1.83$	$12.72 \pm 4.14$	<b><math>5.00 \pm 1.47</math></b>	$15.49 \pm 2.14$	$13.32 \pm 1.08$	$18.61 \pm 1.63$

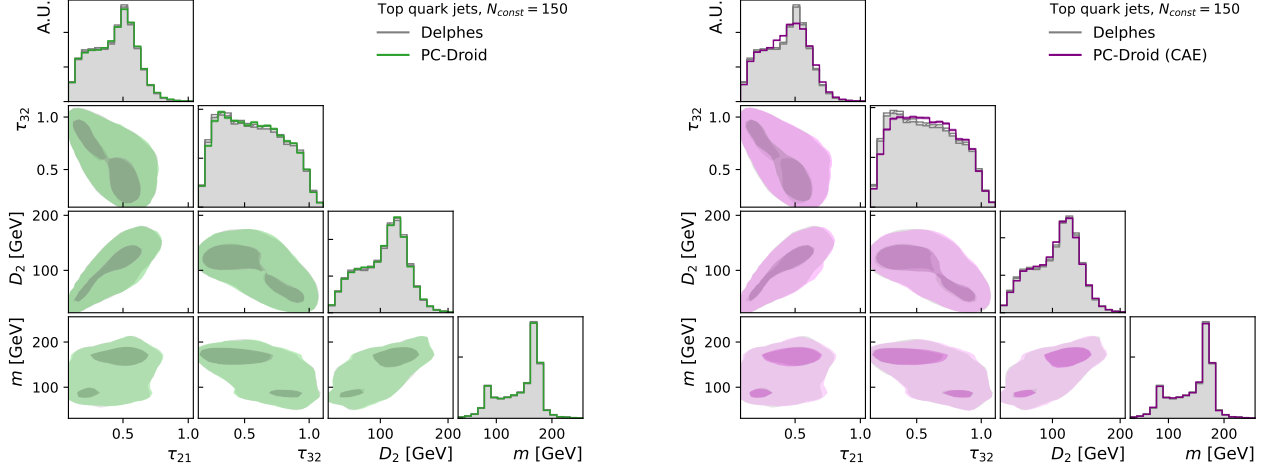


FIG. 7: Mass and substructure distributions of the generated top jets with up to 150 constituents. The diagonal consists of the marginals of the distributions and the off-diagonal elements contain the joint distributions.

TABLE III: Top jet selection efficiency and gluon rejection efficiency (both in %) for the Delphes simulation and jets generated with PC-Droid and EPiC-GAN. Jets are generated with up to 150 constituents.

Model	Top Efficiency	Gluon Rejection
Delphes	$70.0 \pm 0.36$	$83.6 \pm 0.17$
PC-Droid	$70.0 \pm 0.36$	$83.7 \pm 0.17$
PC-Droid (CAE)	$69.2 \pm 0.36$	$83.8 \pm 0.17$
EPiC-GAN	$65.1 \pm 0.34$	$86.5 \pm 0.16$

using the  $\tau_{32}$  and  $D_{12}$  variables. We do not use the combined jet mass as a discriminating variable as we choose to focus on the substructure of the jets. The cuts are selected to maximise the signal significance ( $S/\sqrt{B}$ ) at a signal efficiency targeting 70%. The efficiencies for test set and generated jets are summarized in Table III. Notably, the efficiencies of PC-Droid are very close to those of Delphes, while EPiC-GAN exhibits lower efficiency for both classes of jet. The decision boundaries are shown in Fig. 8, which also shows that the variables are better modelled by PC-Droid.

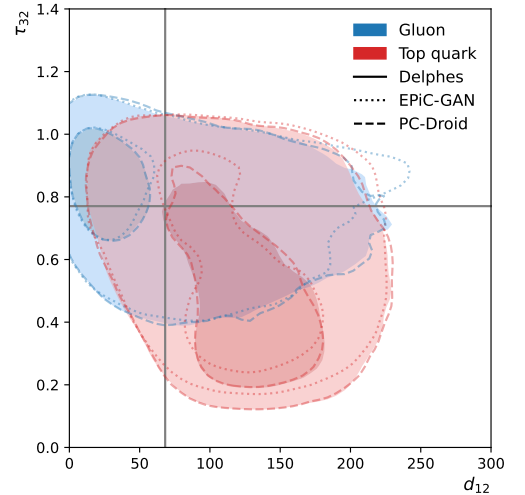


FIG. 8: Decision boundaries for the 2D cut based tagger using  $d_{12}$  and  $\tau_{32}$  for top and gluon jets with up to 150 constituents.

### C. Conditional adherence

As PC-Droid is a conditional generative model it is of interest to see if the model generates jets with kinematics following the conditioning values. To test this we look at the difference between the reconstructed jet kinematics and the target conditions for mass and  $p_T$  in Fig. 9.

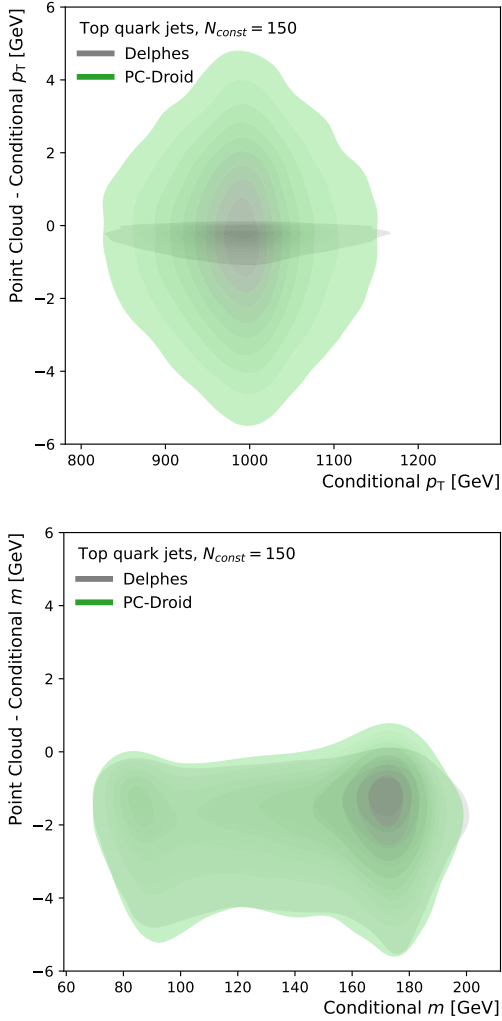


FIG. 9: The correlation between the conditional and point cloud kinematics on top jets with up to 150 constituents. The  $y$ -axis, shows the difference between the two variables.

It is important to note that the exact jet kinematics from simulation are used for the *conditional kinematics* whilst the *point cloud kinematics* are recalculated from the preprocessed jet constituents. These different approaches result in slight discrepancies between the conditional and point cloud variables, even for the Delphes dataset, though it is minor. Furthermore, the original jets may have had even more than 150 constituents when the kinematics were calculated, which is why the shift in mass and  $p_T$  is negative.

For the mass plot in Fig. 9 we see PC-Droid has a near identical spread compared to Delphes. For  $p_T$  there is slightly more variation as the residual magnitudes are higher, but PC-Droid is within 0.4% of the target.

#### D. Consistency models

All diffusion models involve a balance between the number of iterations used during generation and the quality of the final sample. With consistency models, although the samples are not generated with the same fidelity, they are able to produce realistic samples with as few as one iteration step. Furthermore, when restricted to only a few number of steps, they substantially outperform diffusion models.

In order to improve the generation speed and study its impact on the performance, we train a consistency model using the PC-Droid model as the teacher. We use the same training configuration as the original paper [44] with one modification. Instead of using the Heun integration solver to select adjacent points of the ODE, we find DPM2 improves the performance of the consistency model. For generation, we are able to achieve reasonable performance with just a single network pass. When moving to multi-step generation, we observe that the performance saturates after five steps.

The substructure variables for jets produced with the CD model using one-step (CD1) and multi-step (CD5) generation are compared in Fig. 10. The top jet subjet-tiness ratios prove again to be the hardest to reproduce, but the one-shot consistency model also demonstrates an overall smear in the mass.

As the main benefit of consistency models is the improved generation time it is useful to compare the overall trade-off for all models. Figure 11 shows three representative metrics for all models as a function of the generation time for producing top jets with 150 constituents. All scores are calculated with respect to the ideal performance, defined by the Delphes dataset. Our fastest

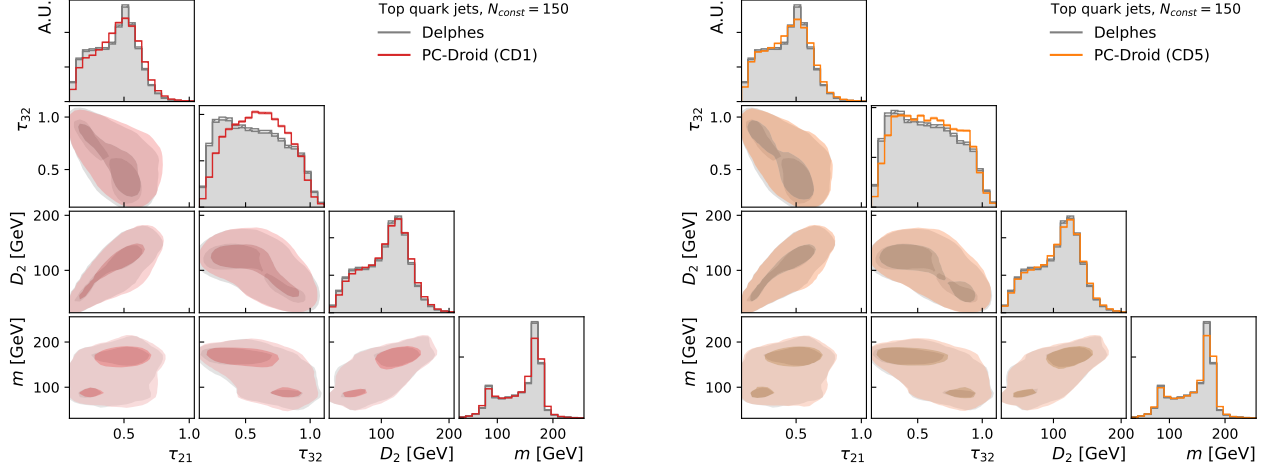


FIG. 10: Mass and substructure distributions of the generated top jets with up to 150 constituents using the CD models. The diagonal consists of the marginals of the distributions and the off-diagonal elements contain the joint distributions.

model (CD1) is around three times slower than EPiC-GAN and suffers from a less accurately reconstructed invariance mass of the jets. However, the FPND score is an order of magnitude closer to the ideal score, with  $\tau_{32}$  comparable between the two. CD5 is a further five times slower than the one-shot generation, but brings improvements to all metrics. The CAE model has a similar FPND to CD5 but notably improves the mass and substructure modelling at the cost of being a further five times slower. Finally the full PC-Droid model is around 250 times slower than EPiC-GAN, but obtains near ideal performance in all but  $W_1^{T_{32}}$ .

In comparison to the progressive distillation models in Ref. [36], our fastest consistency model is more than twice as fast, with performance closer to that achieved by EPiC-GAN. When comparing multi-step distillation approaches, CD5 requires just under 60% the time taken by FPCD8.<sup>4</sup>

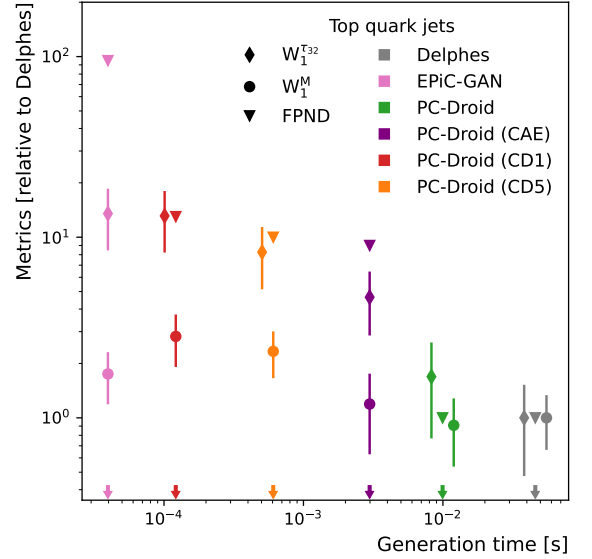


FIG. 11: Performance as a ratio to Delphes as a function of the required generation time for a top jet with up to 150 constituents. The time for Delphes is taken from Ref. [45], all other models are calculated from the average of ten runs each generating a batch of 512 jets using an NVIDIA® GeForce RTX 3080.

<sup>4</sup> Due to different hardware, timing comparisons are calculated with respect to the EPiC-GAN for jets with 150 constituents [36].

#### IV. CONCLUSION

In this work we have introduced an updated version of the PC-JeDi model for generating jets as particle clouds, called PC-Droid. An improved diffusion noise scheduler and training procedure, as well as more modern integration solvers, combine to yield state-of-the-art results across a wide range of metrics. We also consider more jet types and provide a clean and simple method to perform unconditional generation.

We study an additional network architecture to optimise the trade-off between speed and generation quality, and demonstrate the potential of consistency models for one-shot generation. Even with our fastest models we outperform other competing methods across several of the studied metrics.

Due to its success at jet generation, we expect the find-

ings in this work to be similarly competitive at generating other physical point clouds. A natural application is for the simulation of particle showers in calorimeters, which has already seen successful and encouraging performance from the application of diffusion models [32, 33].

#### ACKNOWLEDGEMENTS

The authors would like to acknowledge funding through the SNSF Sinergia grant called "Robust Deep Density Models for High-Energy Particle Physics and Solar Flare Analysis (RODEM)" with funding number CRSII5\_193716 and the SNSF project grant 200020\_212127 called "At the two upgrade frontiers: machine learning and the ITk Pixel detector". They would also like to acknowledge the funding acquired through the Swiss Government Excellence Scholarships for Foreign Scholars.

- 
- [1] L. de Oliveira, M. Paganini, and B. Nachman, Controlling Physical Attributes in GAN-Accelerated Simulation of Electromagnetic Calorimeters, *J. Phys. Conf. Ser.* **1085**, 042017 (2018).
  - [2] M. Paganini, L. de Oliveira, and B. Nachman, Calogan : Simulating 3d high energy particle showers in multilayer electromagnetic calorimeters with generative adversarial networks, *Phys. Rev. D* **97**, 014021 (2018).
  - [3] M. Paganini, L. de Oliveira, and B. Nachman, Accelerating Science with Generative Adversarial Networks: An Application to 3D Particle Showers in Multilayer Calorimeters, *Phys. Rev. Lett.* **120**, 042003 (2018).
  - [4] M. Erdmann, J. Glombitza, and T. Quast, Precise simulation of electromagnetic calorimeter showers using a Wasserstein Generative Adversarial Network, *Comput. Softw. Big Sci.* **3**, 4 (2019).
  - [5] D. Belayneh *et al.*, Calorimetry with deep learning: particle simulation and reconstruction for collider physics, *Eur. Phys. J. C* **80**, 688 (2020).
  - [6] E. Buhmann *et al.*, Getting High: High Fidelity Simulation of High Granularity Calorimeters with High Speed, *Comput. Softw. Big Sci.* **5**, 13 (2021).
  - [7] C. Krause and D. Shih, CaloFlow: Fast and Accurate Generation of Calorimeter Showers with Normalizing Flows, 2106.05285 (2021).
  - [8] C. Krause and D. Shih, CaloFlow II: Even Faster and Still Accurate Generation of Calorimeter Showers with Normalizing Flows, 2110.11377 (2021).
  - [9] The ATLAS Collaboration, AtlFast3: the next generation of fast simulation in ATLAS, *Comput. Softw. Big Sci.* **6**, 7 (2022).
  - [10] The ATLAS Collaboration, Deep generative models for fast photon shower simulation in ATLAS, 2210.06204 (2022).
  - [11] A. Adelmann *et al.*, New directions for surrogate models and differentiable programming for High Energy Physics detector simulation, in *2022 Snowmass Summer Study* (2022) 2203.08806.

- [12] C. Krause, I. Pang, and D. Shih, CaloFlow for CaloChallenge Dataset 1, arXiv:2210.14245 [physics.ins-det] (2022).
- [13] J. Liu, A. Ghosh, D. Smith, P. Baldi, and D. White-son, Generalizing to new calorimeter geometries with Geometry-Aware Autoregressive Models (GAAMs) for fast calorimeter simulation, arXiv:2305.11531 [physics.ins-det] (2023).
- [14] S. Otten *et al.*, Event Generation and Statistical Sampling for Physics with Deep Generative Models and a Density Information Buffer, *Nature Commun.* **12**, 2985 (2021).
- [15] B. Hashemi *et al.*, LHC analysis-specific datasets with Generative Adversarial Networks, 1901.05282 (2019).
- [16] R. Di Sipio *et al.*, DijetGAN: A Generative-Adversarial Network Approach for the Simulation of QCD Dijet Events at the LHC, *JHEP* **08**, 110.
- [17] A. Butter, T. Plehn, and R. Winterhalder, How to GAN LHC Events, *SciPost Phys.* **7**, 075 (2019).
- [18] J. Arjona Martinez *et al.*, Particle Generative Adversarial Networks for full-event simulation at the LHC and their application to pileup description, *J. Phys. Conf. Ser.* **1525**, 012081 (2020).
- [19] C. Gao *et al.*, Event Generation with Normalizing Flows, *Phys. Rev. D* **101**, 076002 (2020).
- [20] Y. Alanazi *et al.*, Simulation of electron-proton scattering events by a Feature-Augmented and Transformed Generative Adversarial Network (FAT-GAN) (2020).
- [21] M. Bellagente *et al.*, Invertible Networks or Partons to Detector and Back Again, *SciPost Phys.* **9**, 074 (2020).
- [22] L. Velasco *et al.*, cFAT-GAN: Conditional Simulation of Electron-Proton Scattering Events with Variate Beam Energies by a Feature Augmented and Transformed Generative Adversarial Network, in *19th IEEE International Conference on Machine Learning and Applications* (2020) pp. 372–375.
- [23] A. Butter and T. Plehn, Generative Networks for LHC events, 2008.08558 (2020).
- [24] J. N. Howard *et al.*, Learning to simulate high energy particle collisions from unlabeled data, *Sci. Rep.* **12**, 7567 (2022).
- [25] G. Quétant *et al.*, Turbo-Sim: a generalised generative model with a physical latent space, arXiv:2112.10629 [cs.LG] (2021).
- [26] J. Ho and T. Salimans, Classifier-free diffusion guidance, 2207.12598 (2022).
- [27] A. Ramesh *et al.*, Hierarchical text-conditional image generation with clip latents, 2204.06125 (2022).
- [28] J. Ho, A. Jain, and P. Abbeel, Denoising diffusion probabilistic models, in *Proceedings of Advances in Neural Information Processing Systems*, Vol. 33 (2020) pp. 6840–6851, 2006.11239.
- [29] A. Q. Nichol and P. Dhariwal, Improved denoising diffusion probabilistic models, in *Proceedings of the 38th International Conference on Machine Learning*, Vol. 139 (2021) pp. 8162–8171, 2102.09672.
- [30] J. Song, C. Meng, and S. Ermon, Denoising diffusion implicit models, 2010.02502 (2020).
- [31] T. Karras *et al.*, Elucidating the design space of diffusion-based generative models, in *Proceedings of Advances in Neural Information Processing Systems* (2022) 2206.00364.
- [32] V. Mikuni and B. Nachman, Score-based generative models for calorimeter shower simulation, *Phys. Rev. D* **106**, 092009 (2022).
- [33] E. Buhmann, S. Diefenbacher, E. Eren, F. Gaede, G. Kasieczka, A. Korol, W. Korcari, K. Krüger, and P. McKeown, CaloClouds: Fast Geometry-Independent Highly-Granular Calorimeter Simulation, arXiv:2305.04847 [physics.ins-det] (2023).
- [34] F. T. Acosta, V. Mikuni, B. Nachman, M. Arratia, K. Barish, B. Karki, R. Milton, P. Karande, and A. Angerami, Comparison of Point Cloud and Image-based Models for Calorimeter Fast Simulation, arXiv:2307.04780 [cs.LG] (2023).
- [35] M. Leigh, D. Sengupta, G. Quétant, J. A. Raine, K. Zoch, and T. Golling, PC-JeDi: Diffusion for Particle Cloud Generation in High Energy Physics, arXiv:2303.05376 [hep-ph] (2023).
- [36] V. Mikuni, B. Nachman, and M. Pettee, Fast Point Cloud Generation with Diffusion Models in High Energy Physics, arXiv:2304.01266 [hep-ph] (2023).
- [37] A. Butter, N. Huetsch, S. P. Schweitzer, T. Plehn, P. Sorrenson, and J. Spinner, Jet Diffusion versus JetGPT – Modern Networks for the LHC, arXiv:2305.10475 [hep-ph] (2023).

- [38] A. Shmakov, K. Greif, M. Fenton, A. Ghosh, P. Baldi, and D. Whiteson, End-To-End Latent Variational Diffusion Models for Inverse Problems in High Energy Physics, arXiv:2305.10399 [hep-ex] (2023).
- [39] V. Mikuni and B. Nachman, High-dimensional and Permutation Invariant Anomaly Detection, arXiv:2306.03933 [hep-ph] (2023).
- [40] L. Yang, Z. Zhang, Y. Song, S. Hong, R. Xu, Y. Zhao, W. Zhang, B. Cui, and M.-H. Yang, Diffusion models: A comprehensive survey of methods and applications, arXiv:2209.00796 [cs.LG] (2023).
- [41] J. Gui, Z. Sun, Y. Wen, D. Tao, and J. Ye, A review on generative adversarial networks: Algorithms, theory, and applications, arXiv:2001.06937 [cs.LG] (2020).
- [42] C. Lu *et al.*, Dpm-solver: A fast ode solver for diffusion probabilistic model sampling in around 10 steps, 2206.00927 (2022).
- [43] C. Lu *et al.*, Dpm-solver++: Fast solver for guided sampling of diffusion probabilistic models, 2211.01095 (2022).
- [44] Y. Song, P. Dhariwal, M. Chen, and I. Sutskever, Consistency models, arXiv:2303.01469 [cs.LG] (2023).
- [45] R. Kansal *et al.*, Particle cloud generation with message passing generative adversarial networks, in *Proceedings of Advances in Neural Information Processing Systems*, Vol. 34 (2021) pp. 23858–23871, 2106.11535.
- [46] R. Kansal *et al.*, Jetnet, 10.5281/zenodo.6975118 (2022).
- [47] R. Kansal *et al.*, Jetnet150, 10.5281/zenodo.6302240 (2022).
- [48] E. Buhmann, G. Kasieczka, and J. Thaler, EPiC-GAN: Equivariant Point Cloud Generation for Particle Jets, 2301.08128 (2023).
- [49] Y. Song *et al.*, Score-based generative modeling through stochastic differential equations, in *Proceedings of the International Conference on Learning Representations* (2021) 2011.13456.
- [50] V. Mnih, K. Kavukcuoglu, D. Silver, A. Graves, I. Antonoglou, D. Wierstra, and M. Riedmiller, Playing atari with deep reinforcement learning, arXiv:1312.5602 [cs.LG] (2013).
- [51] T. Lillicrap *et al.*, Continuous control with deep reinforcement learning, in *International Conference on Learning Representations* (2016).
- [52] T. Salimans and J. Ho, Progressive distillation for fast sampling of diffusion models, in *International Conference on Learning Representations* (2022).
- [53] D. Rezende and S. Mohamed, Variational inference with normalizing flows, in *Proceedings of the 32nd International Conference on Machine Learning*, Vol. 37 (2015) pp. 1530–1538.
- [54] C. Durkan *et al.*, Neural spline flows, in *Proceedings of Advances in Neural Information Processing Systems*, Vol. 32 (Vancouver, Canada, 2019) arXiv:1906.04032 [stat.ML].
- [55] D. P. Kingma and J. Ba, Adam: A method for stochastic optimization, in *Conference Track Proceedings of the 3rd International Conference on Learning Representations* (2015) 1412.6980.
- [56] B. Käch, D. Krücker, I. Melzer-Pellmann, M. Scham, S. Schnake, and A. Verney-Provatas, JetFlow: Generating Jets with Conditioned and Mass Constrained Normalising Flows, arXiv:2211.13630 [hep-ex] (2022).
- [57] B. Käch and I. Melzer-Pellmann, Attention to Mean-Fields for Particle Cloud Generation, arXiv:2305.15254 [hep-ex] (2023).
- [58] J. C. Butcher, *Numerical Methods for Ordinary Differential Equations* (John Wiley and Sons, Ltd, 2016) Chap. 4, pp. 333–387.
- [59] The ATLAS Collaboration, Performance of top-quark and  $W$ -boson tagging with ATLAS in Run 2 of the LHC, Eur. Phys. J. C **79**, 375 (2019), arXiv:1808.07858 [hep-ex].
- [60] The ATLAS Collaboration, *Identification of boosted, hadronically-decaying  $W$  and  $Z$  bosons in  $\sqrt{s} = 13$  TeV Monte Carlo Simulations for ATLAS*, Tech. Rep. (CERN, Geneva, 2015).
- [61] The ATLAS Collaboration, *Identification of boosted, hadronically-decaying  $W$  and  $Z$  bosons in  $\sqrt{s} = 13$  TeV Monte Carlo Simulations for ATLAS*, Tech. Rep. (CERN, Geneva, 2015).

## Appendix A: Additional Material

### 1. Modelling the jet kinematics

Using normalizing flows we can choose to either sample the full suite of jet kinematics along with  $N_{const}$  (Flow- $\vec{p}$ ) or just  $N_{const}$  (Flow- $N$ ) given the jet kinematics. Both Flow- $\vec{p}$  and Flow- $N$  are conditional on PID. It is important to note that these flows are trained independent of PC-Droid as this is a completely orthogonal task. The performance of Flow- $\vec{p}$  is demonstrated in Fig. 12, where

we observe that the marginals and correlations of the conditioning variables are accurately modelled.

We compare the conditional and unconditional models using the full set of metrics in Table IV. Here PC-Droid represents the conditional model, where the  $N_{const}$  and the jet kinematics come from the test set. The other two rows represent using either flow to first sample these variables before passing to the diffusion model. There very little difference in the performance when moving to unconditional generation, and PC-JeDi is still notably outperforming other methods.



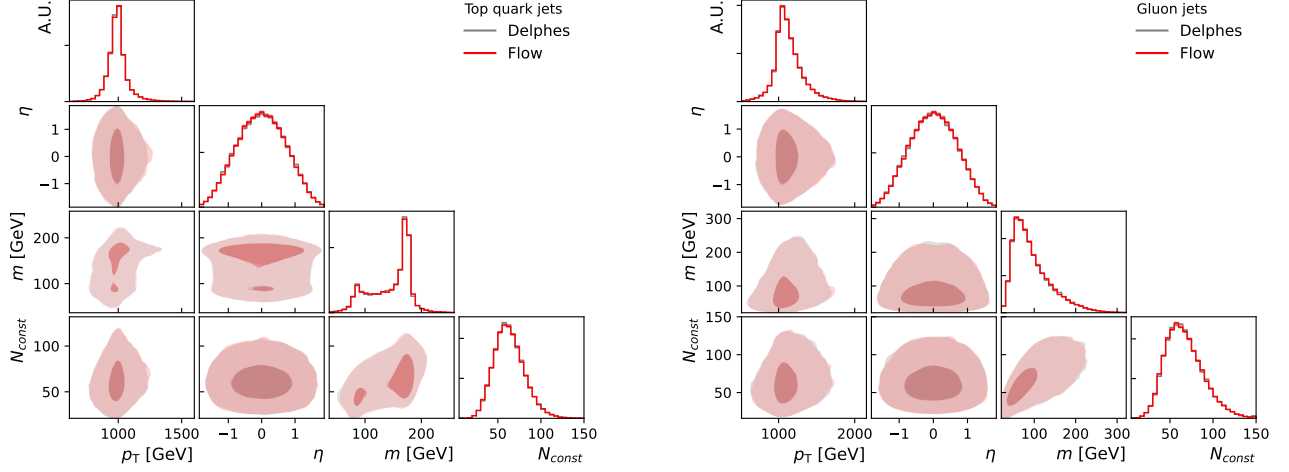


FIG. 12: Marginals of the conditioning variables generated with Flow- $\vec{p}$  (red) compared to Delphes (black) for top and gluon jets with up to 150 constituents.

TABLE IV: Comparison of conditional and unconditional models on jets with up to 150 constituents. Lower is better for all metrics except Cov. The FPNP score is only sensitive to the leading 30 constituents.

Jet	Model	FPND	$W_1^P (\times 10^{-4})$	$W_1^{EFP} (\times 10^{-6})$	$W_1^M (\times 10^{-4})$	$W_1^{T21} (\times 10^{-3})$	$W_1^{T32} (\times 10^{-3})$	$W_1^{D2} (\times 10^{-1})$	MMD ( $\times 10^{-1}$ )	Cov $\uparrow$
Top	Delphes	0.01	$3.03 \pm 0.78$	$14.77 \pm 5.61$	$3.96 \pm 0.94$	$1.78 \pm 0.56$	$2.78 \pm 1.03$	$3.82 \pm 1.54$	0.48	0.58
	PC-Droid	<b>0.01</b>	$5.45 \pm 1.70$	$15.41 \pm 5.38$	<b><math>3.60 \pm 1.20</math></b>	<b><math>2.87 \pm 1.20</math></b>	<b><math>4.70 \pm 1.88</math></b>	<b><math>4.07 \pm 0.85</math></b>	0.49	<b>0.58</b>
	PC-Droid (Flow- $\vec{p}$ )	0.02	$4.95 \pm 1.34$	$17.97 \pm 4.44$	$4.84 \pm 1.18$	$3.40 \pm 1.29$	$5.35 \pm 1.33$	$4.89 \pm 1.05$	<b>0.48</b>	<b>0.58</b>
	PC-Droid (Flow- $N$ )	<b>0.01</b>	<b><math>4.89 \pm 1.47</math></b>	<b><math>14.14 \pm 3.93</math></b>	$3.91 \pm 1.35$	$3.39 \pm 1.28$	$5.28 \pm 1.33$	$4.87 \pm 1.02$	0.49	<b>0.58</b>
Gluon	Delphes	0.01	$3.88 \pm 1.24$	$10.66 \pm 3.30$	$6.04 \pm 2.18$	$2.92 \pm 1.20$	$1.74 \pm 0.45$	$4.65 \pm 1.35$	0.26	0.57
	PC-Droid	<b>0.01</b>	$3.69 \pm 1.35$	$10.30 \pm 4.36$	$5.26 \pm 2.43$	<b><math>3.13 \pm 1.10</math></b>	$2.24 \pm 0.93$	$4.81 \pm 1.27$	<b>0.27</b>	<b>0.55</b>
	PC-Droid (Flow- $\vec{p}$ )	<b>0.01</b>	<b><math>3.63 \pm 1.56</math></b>	$10.63 \pm 2.07$	$6.10 \pm 3.02$	$3.43 \pm 1.19$	$2.24 \pm 0.91$	$4.71 \pm 1.16$	<b>0.27</b>	<b>0.56</b>
	PC-Droid (Flow- $N$ )	0.02	$4.01 \pm 1.22$	<b><math>9.74 \pm 2.53</math></b>	<b><math>4.90 \pm 1.54</math></b>	$3.40 \pm 1.21$	<b><math>2.20 \pm 0.90</math></b>	<b><math>4.71 \pm 1.14</math></b>	<b>0.27</b>	<b>0.55</b>
Quark	Delphes	0.01	$4.87 \pm 1.98$	$7.38 \pm 2.13$	$4.54 \pm 1.69$	$2.79 \pm 0.89$	$1.92 \pm 0.60$	$4.04 \pm 0.96$	0.17	0.54
	PC-Droid	<b>0.01</b>	$5.96 \pm 1.76$	<b><math>6.13 \pm 1.91</math></b>	$4.42 \pm 1.86$	$3.58 \pm 0.96$	<b><math>1.88 \pm 0.62</math></b>	<b><math>3.78 \pm 1.30</math></b>	<b>0.17</b>	0.55
	PC-Droid (Flow- $\vec{p}$ )	<b>0.01</b>	$7.18 \pm 2.33$	$6.46 \pm 1.42$	$4.83 \pm 1.41$	$2.95 \pm 1.04$	$2.26 \pm 0.79$	$4.62 \pm 1.12$	0.18	<b>0.55</b>
	PC-Droid (Flow- $N$ )	<b>0.01</b>	<b><math>5.52 \pm 1.86</math></b>	$6.40 \pm 1.82$	<b><math>4.19 \pm 1.07</math></b>	<b><math>2.92 \pm 1.05</math></b>	$2.26 \pm 0.78$	$4.61 \pm 1.10$	<b>0.17</b>	0.55
W Boson	Delphes	—	$3.86 \pm 1.16$	$1.87 \pm 0.51$	$1.73 \pm 0.47$	$2.79 \pm 0.83$	$3.19 \pm 1.31$	$4.56 \pm 1.60$	0.18	0.56
	PC-Droid	—	<b><math>3.32 \pm 0.98</math></b>	<b><math>1.49 \pm 0.38</math></b>	$1.72 \pm 0.75$	$3.33 \pm 1.12$	<b><math>2.14 \pm 0.61</math></b>	<b><math>3.45 \pm 0.94</math></b>	<b>0.19</b>	0.55
	PC-Droid (Flow- $\vec{p}$ )	—	$3.77 \pm 1.08$	$2.07 \pm 0.50$	$2.27 \pm 0.58$	<b><math>3.02 \pm 1.02</math></b>	$3.27 \pm 1.04$	$3.91 \pm 1.20$	<b>0.19</b>	<b>0.56</b>
	PC-Droid (Flow- $N$ )	—	$3.62 \pm 0.98$	$1.82 \pm 0.44$	<b><math>1.70 \pm 0.58</math></b>	$3.08 \pm 1.01$	$3.31 \pm 1.06$	$3.95 \pm 1.20$	<b>0.19</b>	0.55
Z Boson	Delphes	—	$4.12 \pm 1.57$	$2.10 \pm 0.54$	$2.19 \pm 0.77$	$3.10 \pm 1.49$	$2.00 \pm 0.59$	$3.78 \pm 1.47$	0.20	0.57
	PC-Droid	—	$3.90 \pm 1.32$	$2.01 \pm 0.67$	$1.95 \pm 0.52$	<b><math>2.71 \pm 0.99</math></b>	<b><math>2.22 \pm 0.62</math></b>	<b><math>3.00 \pm 0.78</math></b>	<b>0.21</b>	<b>0.56</b>
	PC-Droid (Flow- $\vec{p}$ )	—	<b><math>3.62 \pm 1.07</math></b>	$1.86 \pm 0.39$	$1.95 \pm 0.69$	$3.03 \pm 1.05$	$2.34 \pm 0.67$	$4.01 \pm 1.08$	<b>0.21</b>	<b>0.56</b>
	PC-Droid (Flow- $N$ )	—	$4.46 \pm 1.48$	<b><math>1.81 \pm 0.51</math></b>	<b><math>1.70 \pm 0.66</math></b>	$3.01 \pm 1.06$	$2.31 \pm 0.67$	$3.95 \pm 1.09$	<b>0.21</b>	0.55

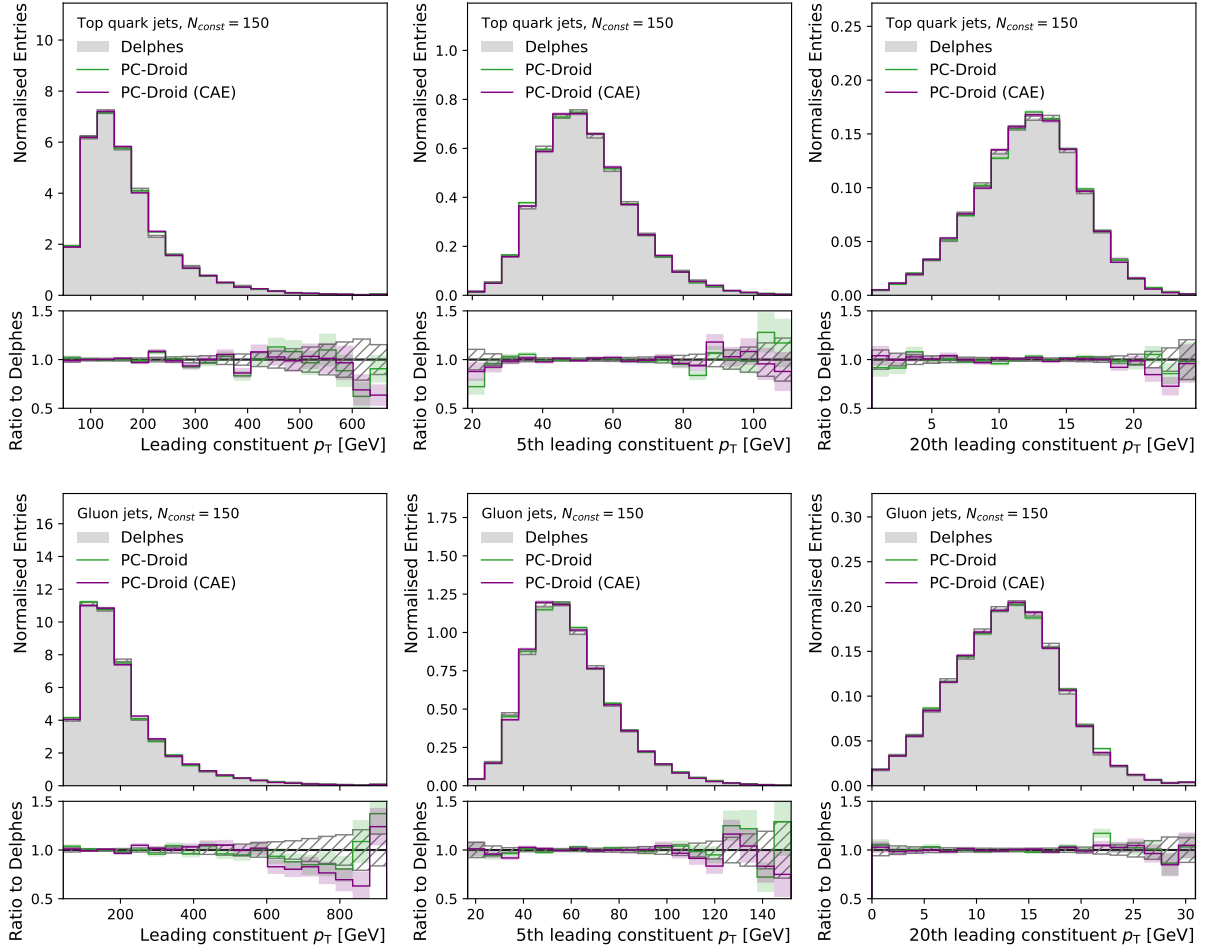


FIG. 13: Comparison of  $p_T$  distributions of the leading, fifth leading, and twentieth leading constituents of the generated top and gluon jets with up to 150 constituents.

TABLE V: Comparison of all models on jets with up to 30 constituents. Upper limit of performance calculated using the Delphes dataset.

Jet	Model	FPND	$W_1^P (\times 10^{-4})$	$W_1^{EFP} (\times 10^{-6})$	$W_1^M (\times 10^{-4})$	$W_1^{T21} (\times 10^{-3})$	$W_1^{T32} (\times 10^{-3})$	$W_1^{D2} (\times 10^{-1})$	MMD ( $\times 10^{-1}$ )	Cov $\uparrow$
Top	Delphes	0.01	$3.98 \pm 1.27$	$8.07 \pm 3.51$	$3.23 \pm 1.07$	$2.01 \pm 0.74$	$2.90 \pm 1.59$	$3.34 \pm 1.03$	0.58	0.58
	MPGAN	0.36	$21.73 \pm 2.02$	$12.80 \pm 4.89$	$6.41 \pm 2.09$	$6.61 \pm 0.92$	$17.41 \pm 2.78$	$11.34 \pm 1.03$	0.59	0.57
	EPiC-GAN	0.32	$20.16 \pm 1.71$	$20.56 \pm 4.37$	$7.41 \pm 1.55$	$11.90 \pm 1.53$	$14.48 \pm 1.01$	$31.05 \pm 3.20$	<b>0.58</b>	0.58
	PC-JeDi	0.15	$12.07 \pm 2.01$	$35.61 \pm 4.92$	$13.64 \pm 3.21$	$4.55 \pm 1.16$	$16.05 \pm 1.31$	$14.12 \pm 1.48$	0.59	0.58
	PC-Droid	<b>0.02</b>	<b><math>5.02 \pm 1.59</math></b>	<b><math>11.59 \pm 3.29</math></b>	<b><math>4.27 \pm 1.39</math></b>	<b><math>2.91 \pm 1.09</math></b>	<b><math>5.14 \pm 1.06</math></b>	<b><math>4.75 \pm 1.26</math></b>	0.59	<b>0.59</b>
	PC-Droid (CD1)	0.12	$6.32 \pm 1.71$	$27.06 \pm 5.26$	$5.95 \pm 1.29$	$15.43 \pm 1.27$	$34.66 \pm 1.57$	$25.08 \pm 1.80$	0.59	<b>0.59</b>
	PC-Droid (CD5)	0.10	$5.75 \pm 1.83$	$20.95 \pm 3.28$	$5.92 \pm 0.79$	$9.14 \pm 1.18$	$26.95 \pm 2.33$	$16.63 \pm 2.60$	0.59	0.58
	FPCD $^\dagger$	0.14	$8 \pm 1^*$	$45 \pm 2$	$17 \pm 1$	—	—	—	<b>0.5*</b>	0.56
Gluon	Delphes	0.01	$3.54 \pm 1.19$	$4.07 \pm 1.27$	$4.39 \pm 1.59$	$3.79 \pm 1.42$	$2.26 \pm 0.51$	$3.72 \pm 1.07$	0.31	0.56
	MPGAN	0.13	$10.26 \pm 1.51$	$8.76 \pm 2.44$	$8.15 \pm 2.10$	$16.83 \pm 2.08$	$25.27 \pm 1.29$	$24.88 \pm 2.91$	0.31	0.54
	EPiC-GAN	1.10	$16.51 \pm 1.98$	$5.48 \pm 1.33$	$5.09 \pm 2.06$	$21.52 \pm 2.54$	$13.80 \pm 1.10$	$22.33 \pm 1.96$	<b>0.30</b>	0.51
	PC-JeDi	0.10	$5.83 \pm 1.44$	$5.68 \pm 1.09$	$5.66 \pm 1.51$	$12.48 \pm 0.98$	$13.32 \pm 0.96$	$10.70 \pm 2.60$	0.31	<b>0.55</b>
	PC-Droid	<b>0.01</b>	<b><math>3.66 \pm 1.07</math></b>	<b><math>4.13 \pm 1.61</math></b>	<b><math>4.48 \pm 1.47</math></b>	<b><math>2.89 \pm 0.80</math></b>	<b><math>1.99 \pm 0.51</math></b>	<b><math>4.14 \pm 1.30</math></b>	<b>0.30</b>	<b>0.55</b>
	PC-Droid (CD1)	0.15	$4.21 \pm 1.02$	$5.94 \pm 2.00$	$5.16 \pm 2.13$	$14.91 \pm 1.01$	$13.22 \pm 0.82$	$11.98 \pm 3.10$	<b>0.30</b>	<b>0.55</b>
	PC-Droid (CD5)	0.17	$5.29 \pm 1.61$	$5.81 \pm 1.46$	$7.27 \pm 3.14$	$11.35 \pm 2.58$	$9.82 \pm 1.04$	$11.56 \pm 2.22$	0.31	<b>0.55</b>
	FPCD $^\dagger$	0.17	$8 \pm 1^*$	$10 \pm 2$	$11 \pm 2$	—	—	—	<b>0.3*</b>	0.55
Quark	Delphes	0.01	$4.58 \pm 1.68$	$3.14 \pm 1.32$	$3.73 \pm 1.10$	$3.23 \pm 1.17$	$1.92 \pm 0.40$	$4.22 \pm 1.74$	0.20	0.55
	MPGAN	0.37	$50.22 \pm 2.05$	$6.91 \pm 1.41$	$6.62 \pm 1.54$	$9.53 \pm 0.45$	$21.62 \pm 0.85$	$21.55 \pm 1.20$	0.21	0.50
	EPiC-GAN	0.47	$39.90 \pm 2.25$	$7.57 \pm 1.53$	$4.97 \pm 1.28$	$18.90 \pm 2.24$	$17.72 \pm 1.07$	$37.23 \pm 2.64$	0.21	0.49
	PC-Droid	<b>0.02</b>	<b><math>4.84 \pm 1.59</math></b>	<b><math>3.29 \pm 1.02</math></b>	<b><math>3.87 \pm 1.55</math></b>	<b><math>5.56 \pm 0.93</math></b>	<b><math>2.82 \pm 0.65</math></b>	<b><math>4.24 \pm 1.17</math></b>	<b>0.20</b>	<b>0.53</b>
	PC-Droid (CD1)	0.29	$5.05 \pm 1.51$	$4.45 \pm 1.52$	$4.89 \pm 2.46$	$15.34 \pm 1.80$	$9.89 \pm 0.84$	$6.81 \pm 1.97$	0.21	0.48
	PC-Droid (CD5)	0.12	$5.96 \pm 1.55$	$5.55 \pm 2.03$	$5.65 \pm 2.27$	$15.30 \pm 2.31$	$7.47 \pm 0.77$	$6.20 \pm 2.11$	0.21	0.48
	FPCD $^\dagger$	0.29	$9 \pm 1^*$	$5 \pm 1^*$	$7 \pm 2^*$	—	—	—	<b>0.2*</b>	0.44
	Delphes	—	$3.70 \pm 0.96$	$1.17 \pm 0.34$	$2.05 \pm 0.63$	$3.12 \pm 1.49$	$3.04 \pm 1.44$	$4.16 \pm 1.52$	0.23	0.58
W Boson	PC-Droid	—	<b><math>3.61 \pm 1.09</math></b>	<b><math>1.02 \pm 0.23</math></b>	<b><math>1.89 \pm 0.83</math></b>	<b><math>3.73 \pm 1.22</math></b>	<b><math>3.63 \pm 1.71</math></b>	<b><math>4.47 \pm 2.07</math></b>	<b>0.23</b>	<b>0.57</b>
	PC-Droid (CD1)	—	$4.58 \pm 1.08$	$3.84 \pm 0.44$	$7.25 \pm 0.41$	$19.08 \pm 1.58$	$9.64 \pm 0.71$	$15.75 \pm 1.64$	0.26	0.56
	PC-Droid (CD5)	—	$4.82 \pm 1.03$	$3.03 \pm 0.30$	$5.22 \pm 0.47$	$7.01 \pm 1.83$	$12.78 \pm 1.34$	$9.65 \pm 1.66$	0.25	<b>0.57</b>
	FPCD $^\dagger$	—	$7.0 \pm 0.8$	$4.8 \pm 0.2$	$11 \pm 0.6$	—	—	—	<b>0.2*</b>	0.55
	Delphes	—	$3.90 \pm 1.09$	$1.36 \pm 0.40$	$2.05 \pm 0.71$	$2.99 \pm 0.95$	$2.18 \pm 0.64$	$3.47 \pm 1.10$	0.26	0.57
Z Boson	PC-Droid	—	<b><math>4.48 \pm 1.26</math></b>	<b><math>1.68 \pm 0.52</math></b>	<b><math>1.95 \pm 0.45</math></b>	<b><math>3.35 \pm 1.11</math></b>	<b><math>3.54 \pm 1.24</math></b>	<b><math>3.71 \pm 0.83</math></b>	<b>0.26</b>	<b>0.57</b>
	PC-Droid (CD1)	—	$5.33 \pm 1.40$	$4.84 \pm 0.45$	$8.11 \pm 1.16$	$18.60 \pm 1.65$	$9.30 \pm 0.79$	$17.43 \pm 1.98$	0.29	0.56
	PC-Droid (CD5)	—	$4.48 \pm 1.03$	$3.94 \pm 0.48$	$6.70 \pm 1.17$	$8.78 \pm 1.87$	$13.60 \pm 1.27$	$9.38 \pm 1.20$	0.28	<b>0.57</b>
	FPCD $^\dagger$	—	$6.5 \pm 1.0$	$16.5 \pm 0.4$	$11.1 \pm 0.4$	—	—	—	<b>0.2*</b>	0.55
	Delphes	—	$3.90 \pm 1.09$	$1.36 \pm 0.40$	$2.05 \pm 0.71$	$2.99 \pm 0.95$	$2.18 \pm 0.64$	$3.47 \pm 1.10$	0.26	0.57

$^\dagger$ Values taken from Ref. [36]; substructure metrics not available for this approach and the statistical uncertainty calculation may differ.

\*Precision only available up to one significant figure.

TABLE VI: Comparison of all models on jets with up to 150 constituents. Upper limit of performance calculated using the Delphes dataset.

Jet	Model	FPND	$W_1^P (\times 10^{-4})$	$W_1^{EFP} (\times 10^{-6})$	$W_1^M (\times 10^{-4})$	$W_1^{T21} (\times 10^{-3})$	$W_1^{T32} (\times 10^{-3})$	$W_1^{D2} (\times 10^{-1})$	MMD ( $\times 10^{-1}$ )	Cov $\uparrow$
Top	Delphes	0.01	$3.03 \pm 0.78$	$14.77 \pm 5.61$	$3.96 \pm 0.94$	$1.78 \pm 0.56$	$2.78 \pm 1.03$	$3.82 \pm 1.54$	0.48	0.58
	EPiC-GAN	0.95	$36.70 \pm 1.80$	$30.29 \pm 5.01$	$6.93 \pm 1.49$	$13.28 \pm 1.80$	$37.56 \pm 1.92$	$19.03 \pm 2.40$	0.58	0.57
	PC-Droid	<b>0.01</b>	$5.45 \pm 1.70$	<b><math>15.41 \pm 5.38</math></b>	<b><math>3.60 \pm 1.20</math></b>	<b><math>2.87 \pm 1.20</math></b>	<b><math>4.70 \pm 1.88</math></b>	<b><math>4.07 \pm 0.85</math></b>	<b>0.49</b>	0.58
	PC-Droid (CAE)	0.09	<b><math>4.93 \pm 1.58</math></b>	$17.97 \pm 4.15$	$4.72 \pm 1.93$	$6.30 \pm 1.00$	$12.94 \pm 1.42$	$6.98 \pm 1.04$	<b>0.49</b>	0.57
	PC-Droid (CD1)	0.13	$6.62 \pm 1.49$	$55.49 \pm 6.99$	$11.18 \pm 2.44$	$19.04 \pm 1.61$	$36.48 \pm 1.67$	$18.60 \pm 3.00$	0.57	<b>0.59</b>
	PC-Droid (CD5)	0.10	$6.78 \pm 1.76$	$54.25 \pm 5.27$	$9.24 \pm 1.53$	$7.53 \pm 0.79$	$22.98 \pm 1.58$	$10.46 \pm 2.84$	0.55	0.58
	FPCD $^\dagger$	—	$9 \pm 1^*$	$86 \pm 2$	$17 \pm 1$	—	—	—	0.5*	0.57
Gluon	Delphes	0.01	$3.88 \pm 1.24$	$10.66 \pm 3.30$	$6.04 \pm 2.18$	$2.92 \pm 1.20$	$1.74 \pm 0.45$	$4.65 \pm 1.35$	0.26	0.57
	EPiC-GAN	0.54	$32.22 \pm 1.83$	$12.72 \pm 4.14$	<b><math>5.00 \pm 1.47</math></b>	$15.49 \pm 2.14$	$13.32 \pm 1.08$	$18.61 \pm 1.63$	0.32	0.53
	PC-Droid	<b>0.01</b>	<b><math>3.69 \pm 1.35</math></b>	<b><math>10.30 \pm 4.36</math></b>	$5.26 \pm 2.43$	<b><math>3.13 \pm 1.10</math></b>	<b><math>2.24 \pm 0.93</math></b>	<b><math>4.81 \pm 1.27</math></b>	<b>0.27</b>	0.55
	PC-Droid (CAE)	0.02	$4.30 \pm 1.48$	$11.31 \pm 3.46$	$5.37 \pm 2.02$	$3.24 \pm 0.90$	$3.06 \pm 0.91$	$5.02 \pm 1.34$	<b>0.27</b>	<b>0.56</b>
	PC-Droid (CD1)	0.10	$6.54 \pm 1.81$	$21.55 \pm 6.13$	$5.55 \pm 2.76$	$15.33 \pm 2.58$	$10.73 \pm 0.80$	$14.11 \pm 2.93$	0.31	<b>0.56</b>
	PC-Droid (CD5)	0.06	$7.05 \pm 1.74$	$14.91 \pm 5.38$	$7.09 \pm 2.90$	$11.11 \pm 2.23$	$9.04 \pm 0.71$	$14.24 \pm 2.57$	0.31	<b>0.56</b>
	FPCD $^\dagger$	—	$10 \pm 1^*$	$38 \pm 2$	$18 \pm 3$	—	—	—	0.3*	0.55
Quark	Delphes	0.01	$4.87 \pm 1.98$	$7.38 \pm 2.13$	$4.54 \pm 1.69$	$2.79 \pm 0.89$	$1.92 \pm 0.60$	$4.04 \pm 0.96$	0.17	0.54
	EPiC-GAN	0.17	$39.69 \pm 2.67$	$8.19 \pm 3.06$	$5.25 \pm 1.78$	$13.00 \pm 1.85$	$10.35 \pm 0.89$	$24.01 \pm 2.20$	0.19	0.51
	PC-Droid	<b>0.01</b>	$5.96 \pm 1.76$	<b><math>6.13 \pm 1.91</math></b>	$4.42 \pm 1.86$	$3.58 \pm 0.96$	<b><math>1.88 \pm 0.62</math></b>	<b><math>3.78 \pm 1.30</math></b>	<b>0.17</b>	<b>0.55</b>
	PC-Droid (CAE)	0.02	<b><math>4.75 \pm 1.39</math></b>	$7.43 \pm 2.85$	$5.21 \pm 1.76$	<b><math>3.09 \pm 0.82</math></b>	$1.96 \pm 0.61$	$3.85 \pm 0.68$	0.18	<b>0.55</b>
	PC-Droid (CD1)	0.27	$7.74 \pm 2.21$	$9.90 \pm 2.69$	$6.50 \pm 1.87$	$13.56 \pm 1.89$	$9.22 \pm 0.60$	$6.30 \pm 1.85$	0.21	0.54
	PC-Droid (CD5)	0.15	$9.87 \pm 2.07$	$7.87 \pm 2.19$	<b><math>4.14 \pm 1.54</math></b>	$12.32 \pm 1.65$	$6.41 \pm 0.71$	$10.25 \pm 2.08$	0.21	0.54
	FPCD $^\dagger$	—	$9.5 \pm 1.4$	$8.2 \pm 1.2$	$5.0 \pm 1.1$	—	—	—	0.2*	0.53
W Boson	Delphes	—	$3.86 \pm 1.16$	$1.87 \pm 0.51$	$1.73 \pm 0.47$	$2.79 \pm 0.83$	$3.19 \pm 1.31$	$4.56 \pm 1.60$	0.18	0.56
	PC-Droid	—	<b><math>3.32 \pm 0.98</math></b>	<b><math>1.49 \pm 0.38</math></b>	<b><math>1.72 \pm 0.75</math></b>	<b><math>3.33 \pm 1.12</math></b>	<b><math>2.14 \pm 0.61</math></b>	<b><math>3.45 \pm 0.94</math></b>	<b>0.19</b>	0.55
	PC-Droid (CAE)	—	$4.43 \pm 1.10$	$2.07 \pm 0.63$	$2.36 \pm 0.51$	$4.58 \pm 1.48$	$2.99 \pm 0.88$	$3.91 \pm 1.15$	<b>0.19</b>	0.55
	PC-Droid (CD1)	—	$5.06 \pm 1.16$	$6.47 \pm 0.89$	$12.80 \pm 0.93$	$26.98 \pm 1.57$	$10.64 \pm 0.73$	$21.07 \pm 2.23$	0.25	<b>0.56</b>
	PC-Droid (CD5)	—	$6.25 \pm 1.07$	$4.40 \pm 0.62$	$8.28 \pm 0.43$	$8.07 \pm 1.48$	$13.30 \pm 1.44$	$12.60 \pm 1.05$	0.24	<b>0.56</b>
	FPCD $^\dagger$	—	$8 \pm 1^*$	$6.5 \pm 0.3$	$13.5 \pm 0.3$	—	—	—	0.2*	0.54
Z Boson	Delphes	—	$4.12 \pm 1.57$	$2.10 \pm 0.54$	$2.19 \pm 0.77$	$3.10 \pm 1.49$	$2.00 \pm 0.59$	$3.78 \pm 1.47$	0.20	0.57
	PC-Droid	—	<b><math>3.90 \pm 1.32</math></b>	<b><math>2.01 \pm 0.67</math></b>	<b><math>1.95 \pm 0.52</math></b>	<b><math>2.71 \pm 0.99</math></b>	<b><math>2.22 \pm 0.62</math></b>	<b><math>3.00 \pm 0.78</math></b>	<b>0.21</b>	<b>0.56</b>
	PC-Droid (CAE)	—	$4.82 \pm 1.32$	$2.27 \pm 0.68$	$1.96 \pm 0.47$	$3.83 \pm 0.91$	$3.10 \pm 1.00$	$3.61 \pm 1.24$	<b>0.21</b>	0.55
	PC-Droid (CD1)	—	$5.04 \pm 0.94$	$6.57 \pm 0.73$	$12.20 \pm 0.53$	$22.78 \pm 2.07$	$9.32 \pm 0.67$	$19.40 \pm 2.78$	0.27	<b>0.56</b>
	PC-Droid (CD5)	—	$5.41 \pm 1.21$	$6.16 \pm 0.74$	$7.99 \pm 0.45$	$6.39 \pm 1.28$	$15.49 \pm 1.23$	$11.50 \pm 1.89$	0.26	<b>0.56</b>
	FPCD $^\dagger$	—	$7 \pm 1^*$	$8.2 \pm 0.4$	$14.2 \pm 0.3$	—	—	—	<b>0.2*</b>	0.55

$^\dagger$ Values taken from Ref. [36]; substructure metrics not available for this approach and the statistical uncertainty calculation may differ.

\*Precision only available up to one significant figure.